Spider toxin inhibits gating pore currents underlying periodic paralysis

Roope Männikkö[a,1,2], Zakhar O. Shenkarev[b,c,1], Michael G. Thor[a], Antonina A. Berkut[b,c], Mikhail Yu Myshkin[b,c], Alexander S. Paramonov[b], Dmitrii S. Kulbatskii[b,d], Dmitry A. Kuzmin[e], Marisol Sampedro Castañeda[a], Louise King[a], Emma R. Wilson[a], Ekaterina N. Lyukmanova[b,c,d], Mikhail P. Kirpichnikov[b,d], Stephanie Schorge[e], Frank Bosmans[f,g], Michael G. Hanna[a], Dimitri M. Kullmann[e], and Alexander A. Vassilevski[b,c,2]

[a]MRC Centre for Neuromuscular Diseases, Department of Molecular Neuroscience, UCL Institute of Neurology, WC1N 3BG London, United Kingdom; [b]Shemyakin–Ovchinnikov Institute of Bioorganic Chemistry, Russian Academy of Sciences, 117997 Moscow, Russia; [c]Department of Biological and Medical Physics, Moscow Institute of Physics and Technology (State University), 117303 Moscow, Russia; [d]Biological Faculty, Lomonosov Moscow State University, 119991 Moscow, Russia; [e]Department of Clinical and Experimental Epilepsy, UCL Institute of Neurology, WC1N 3BG London, United Kingdom; [f]Department of Physiology, Johns Hopkins University School of Medicine; Baltimore, MD 21205; and [g]Solomon H. Snyder Department of Neuroscience, Johns Hopkins University School of Medicine, Baltimore, MD 21205

Edited by Bruce P. Bean, Harvard Medical School, Boston, MA, and approved March 9, 2018 (received for review November 19, 2017)

Gating pore currents through the voltage-sensing domains (VSDs) of the skeletal muscle voltage-gated sodium channel $Na_V1.4$ underlie hypokalemic periodic paralysis (HypoPP) type 2. Gating modifier toxins target ion channels by modifying the function of the VSDs. We tested the hypothesis that these toxins could function as blockers of the pathogenic gating pore currents. We report that a crab spider toxin Hm-3 from *Heriaeus melloteei* can inhibit gating pore currents due to mutations affecting the second arginine residue in the S4 helix of VSD-I that we have found in patients with HypoPP and describe here. NMR studies show that Hm-3 partitions into micelles through a hydrophobic cluster formed by aromatic residues and reveal complex formation with VSD-I through electrostatic and hydrophobic interactions with the S3b helix and the S3–S4 extracellular loop. Our data identify VSD-I as a specific binding site for neurotoxins on sodium channels. Gating modifier toxins may constitute useful hits for the treatment of HypoPP.

hypokalemic periodic paralysis | channelopathy | sodium channel | neurotoxin | gating modifier

Hypokalemic periodic paralysis (HypoPP) is characterized by episodes of muscle weakness or paralysis associated with reduced serum potassium levels (1). Attacks often begin in adolescence, range from mild and limited to severe full-body paralysis, and last from hours to days. Many patients with HypoPP develop permanent muscle weakness and require mobility aids later in life (2). Patients with HypoPP are counseled to avoid known triggers, while acetazolamide and other carbonic anhydrase inhibitors may help prevent episodes of periodic paralysis. However, these drugs have no effect or even worsen symptoms in some patients (3).

The resting membrane potential of muscle fibers from patients with HypoPP is excessively depolarized, leading to inactivation of voltage-gated sodium channels, inexcitability, and paralysis of the muscle (4). Mutations in the skeletal muscle voltage-gated sodium ($Na_V1.4$) and calcium ($Ca_V1.1$) channel genes, *SCN4A* and *CACNA1S*, are associated with HypoPP (5, 6). $Na_V1.4$ and $Ca_V1.1$ are responsible for excitability and excitation/contraction coupling in the muscle, respectively, and the molecular pathomechanism of HypoPP is similar for both channels despite their different role and selectivity (6). Mutations found in patients with HypoPP affect arginine residues in the S4 helices of the voltage-sensing domains (VSDs) of $Ca_V1.1$ (HypoPP type 1) or $Na_V1.4$ (HypoPP type 2).

Na_V and Ca_V channels are composed of four homologous repeats (Fig. 1*A*), each closely related to a subunit of voltage-gated potassium channels (K_Vs). Each repeat consists of six transmembrane α-helices (S1–S6) and contains a VSD formed by helices S1–S4. The central (main) pore is formed by helices S5–S6 from all four repeats (7) (Fig. 1*B*). Arginine residues in the S4 helices reposition relative to a hydrophobic charge transfer center when the transmembrane voltage changes (7, 8) (Fig. 1*C*). Upon depolarization, the S4 segment moves to the extracellular side of the membrane ("up" state), while hyperpolarization pulls it to the intracellular side ("down" state). Up and down conformations of the VSDs stabilize the open and closed states of the pore domain, respectively. The S4 helix moves within a structure called the gating pore that is formed by the VSD. When an S4 arginine is mutated, ions may leak through the gating pore (9, 10). This current is known as gating pore or ω-current (I_{GP}) that flows in addition to the main pore or α-current (I_{Na}) and underlies the abnormal depolarization of HypoPP muscles (4). HypoPP-associated I_{GP}s have been described in $Na_V1.4$ channels with mutations in VSD-I (11), VSD-II (12–14), and VSD-III (15–17), but not in VSD-IV (15, 18) (Fig. 1*A*). I_{GP}s are voltage-dependent; for example, a mutation in one of the two outermost arginines (R1 and R2) of VSD-II results in I_{GP} in the down state of the voltage sensor (12–14). In contrast, a mutation of the third arginine (R3) in VSD-II results in I_{GP} when the voltage sensor is in the up state (19).

Many toxins exert their effects by targeting ion channel function either by directly blocking ion permeation through the channel

Significance

Voltage-gated ion channels contain domains that have discrete functionalities. The central pore domain allows current flow and provides ion selectivity, whereas peripherally located voltage-sensing domains (VSDs) are needed for voltage-dependent gating. Certain mutations trigger a leak current through VSDs, known as gating pore current. Hypokalemic periodic paralysis (HypoPP) type 2 is caused by mutations in the skeletal muscle voltage-gated sodium channel $Na_V1.4$ that neutralize positive charges in S4 voltage-sensing segments of VSDs. We show that Hm-3 toxin from the crab spider *Heriaeus melloteei* inhibits gating pore currents through such mutant channels. We propose that Hm-3 and similar toxins may constitute useful hits in developing gating pore current inhibitors and HypoPP therapy.

Author contributions: R.M., Z.O.S., D.A.K., F.B., M.G.H., D.M.K., and A.A.V. designed research; R.M., M.G.T., A.A.B., M.Y.M., A.S.P., D.S.K., M.S.C., L.K., E.R.W., and F.B. performed research; R.M., Z.O.S., E.N.L., M.P.K., S.S., F.B., M.G.H., D.M.K., and A.A.V. contributed new reagents/analytic tools; R.M., Z.O.S., M.G.T., A.A.B., M.Y.M., M.S.C., L.K., E.R.W., E.N.L., S.S., F.B., D.M.K., and A.A.V. analyzed data; and R.M., Z.O.S., A.A.B., D.A.K., M.S.C., F.B., and A.A.V. wrote the paper.

The authors declare no conflict of interest.

This article is a PNAS Direct Submission.

[1]R.M. and Z.O.S. contributed equally to this work.

[2]To whom correspondence may be addressed. Email: r.mannikko@ucl.ac.uk or avas@ibch.ru.

This article contains supporting information online at www.pnas.org/lookup/suppl/doi:10.1073/pnas.1720185115/-/DCSupplemental.

Published online April 10, 2018.

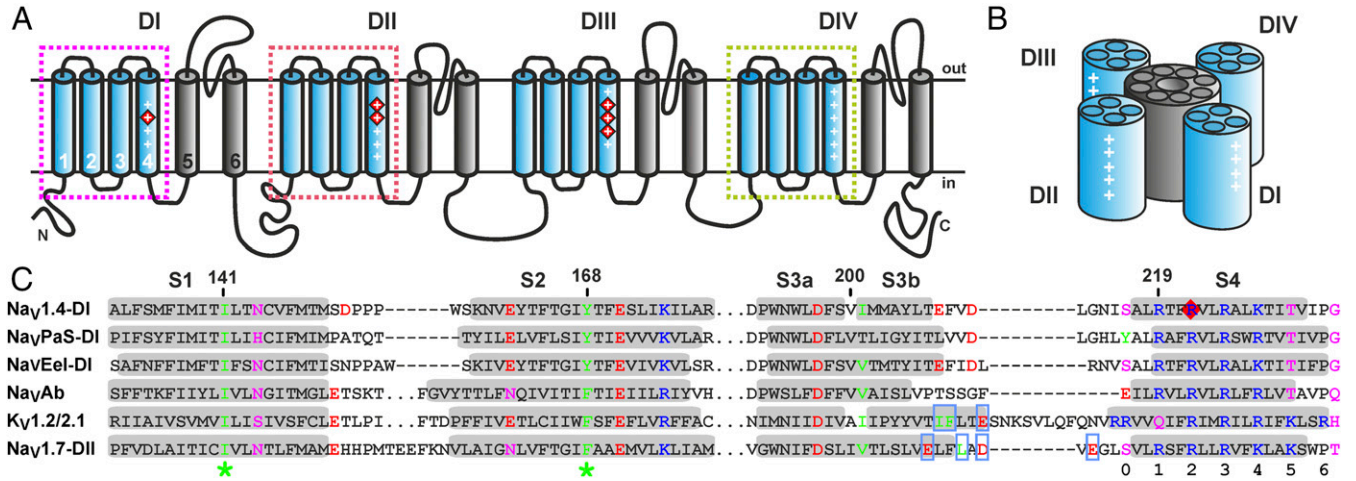

Fig. 1. Na$_V$ channel organization and Na$_V$1.4 VSD-I sequence comparison with other voltage-gated channels. (*A*) Transmembrane topology of Na$_V$ channels. The S1–S4 helices are in blue, and the S5–S6 helices are in gray. Gating charges are marked by "+" signs, and those neutralized in HypoPP are marked by red diamonds. Colored frames indicate VSDs specifically targeted by gating modifier toxins, VSD-I studied by us is shown by magenta. (*B*) Spatial organization of Na$_V$ channels with one pore domain and four VSDs. (*C*) Alignment of Na$_V$1.4 VSD-I with VSDs of other Na$_V$ and K$_V$ channels. Conserved aromatic/hydrophobic, charged, and polar residues are color-coded. Transmembrane segments are highlighted by gray background. The gating charge transfer center is marked by green asterisks. Conserved charged residues in the S4 helix are numbered. Mutation of R222 (red diamond) is associated with HypoPP. Residues of K$_V$1.2/2.1 and Na$_V$1.7-DII responsible for the interaction with hanatoxin (34) and huwentoxin-IV (35), respectively, are boxed. D, domain.

pore or by modifying channel gating. The gating modifier toxins target ion channels by binding to VSD-II (site 4) or VSD-IV (site 3) (20) (Fig. 1 *A* and *C*). We tested the hypothesis that these toxins could inhibit the HypoPP I_{GP} at Na$_V$1.4 VSDs. Our data identify a crab spider toxin as an inhibitor of pathogenic I_{GP} and VSD-I as a specific binding site for sodium channel toxins. We also report an NMR study of structural interactions between toxin and Na$_V$ channel.

Results

Properties of I_{Na} in p.R222W Channels. The p.R222W mutation was found in patients with HypoPP (5), but its molecular pathomechanism was not described. We studied I_{Na} properties of the p.R222W channel in HEK293 cells (Fig. S1 *A–H*). The current density of p.R222W channels was reduced compared with wild-type channels ($P < 0.001$ at 0 mV), whereas the voltage of half-maximal activation and fast or slow inactivation ($V_{1/2}$; see *SI Materials and Methods*) were unaltered. The slope factors of activation and fast inactivation were less steep ($P < 0.01$) and steeper ($P < 0.001$), respectively, for p.R222W channels compared with wild-type channels. In addition, the time constant of open-state inactivation was increased in p.R222W channels [$P < 0.01$ for $\tau(0)$]. Other parameters of p.R222W channels were unaltered.

Many HypoPP mutants show I_{Na} loss of function (21–23) analogous to reduced current density of p.R222W channels. This may result in hypoexcitability and play a role in the clinical phenotype, but it cannot account for the depolarization observed in muscles from patients with HypoPP (4, 22, 24). The reduced rate of sodium channel inactivation is a gain-of-function property that has been associated with paramyotonia and hyperkalemic periodic paralysis, but not with HypoPP (1, 6). HypoPP is often defined as paralysis without myotonia, arguing that the slowed inactivation kinetics are not contributing to the symptoms experienced by mutation carriers.

Properties of I_{GP} in p.R222W Channels. We next asked if p.R222W mutant channels conducted I_{GP} using the *Xenopus laevis* oocyte expression system (Fig. 2 *A–C*). To isolate I_{GP}, I_{Na} was blocked with 1 μM tetrodotoxin. Leak-subtracted current–voltage data revealed hyperpolarization-activated inward currents for p.R222W channels. The current amplitude at −80 mV was −49 ± 11 nA ($n = 21$) for p.R222W channels and 25 ± 6 nA ($n = 20$) for wild-type channels. Guanidinium increases the amplitude of I_{GP} in channels where an S4 arginine has been substituted (10, 25) and can be used to confirm the presence of I_{GP} caused by such mutations. When half of the extracellular sodium was replaced by guanidinium, the current amplitude at −80 mV increased to −0.8 ± 0.1 μA in cells expressing p.R222W channels, whereas the current in cells expressing wild-type channels was 0 ± 15 nA. For uninjected oocytes, these values were 28 ± 12 nA and 10 ± 3 nA in Na^+ and Na^+/Gn^+, respectively ($n = 4$). These data indicate that p.R222W channels conduct hyperpolarization-activated I_{GP}, similar to channels containing the p.R222G mutation found in another patient with HypoPP and previously shown to conduct I_{GP} (11). The mean current amplitude of p.R222G channels at −80 mV was −138 ± 28 nA in a Na^+ solution and −1.7 ± 0.2 μA in Na^+/Gn^+ solution ($n = 42$).

I_{GP} Inhibition by Hm-3. Hm-3 is a gating modifier toxin from the crab spider *Heriaeus melloteei* (26) and has been hypothesized to exert its effect by acting on the VSDs of Na$_V$ channels (27). We tested whether Hm-3 could inhibit guanidinium-enhanced I_{GP} of p.R222W and p.R222G channels (Fig. 2 *D–F*). Hm-3 inhibited I_{GP} for both mutant channels, with 10 μM Hm-3 suppressing 67 ± 5% of p.R222W currents ($n = 4$) and 64 ± 4% of p.R222G currents ($n = 10$) at −80 mV. The IC_{50} for p.R222G channels measured from noncumulative data was 5.4 ± 0.8 μM at −80 mV. This is more than 10-fold higher than the IC_{50} reported for the I_{Na} of Na$_V$1.4 (27).

VSD-I Specific Effects of Hm-3. We tested the specificity of Hm-3 with a series of mutant channels that conduct I_{GP}: p.R672G (R2, VSD-II), p.R1132Q (R2, VSD-III), p.R219G (R1, VSD-I), and p.R225G (R3, VSD-I). Unlike p.R672G and p.R1132Q, p.R219G and p.R225G have not been identified thus far in patients with HypoPP. Guanidinium substantially increases the amplitude of nonlinear leak currents for all mutant channels (Fig. S1*I*), confirming the presence of I_{GP}. For p.R219G, p.R672G, and p.R1132Q channels, the currents were activated by hyperpolarization similar to p.R222W/G channels. In contrast, in p.R225G, I_{GP} was activated by depolarization, although the presence of guanidinium in the extracellular solution increased the current amplitude at all voltages. Hm-3 (10 μM) did not inhibit I_{GP} of mutant channels activated by hyperpolarization ($n = 4$ for p.R672G and p.R1132Q, $n = 6$ for p.R219G; Fig. 3*A*). Hm-3 (10 μM) inhibited the depolarization-activated I_{GP} of p.R225G channels ($n = 9$; Fig. 3*A*) at voltages negative to 0 mV; the I_{GP} was unaffected at positive voltages.

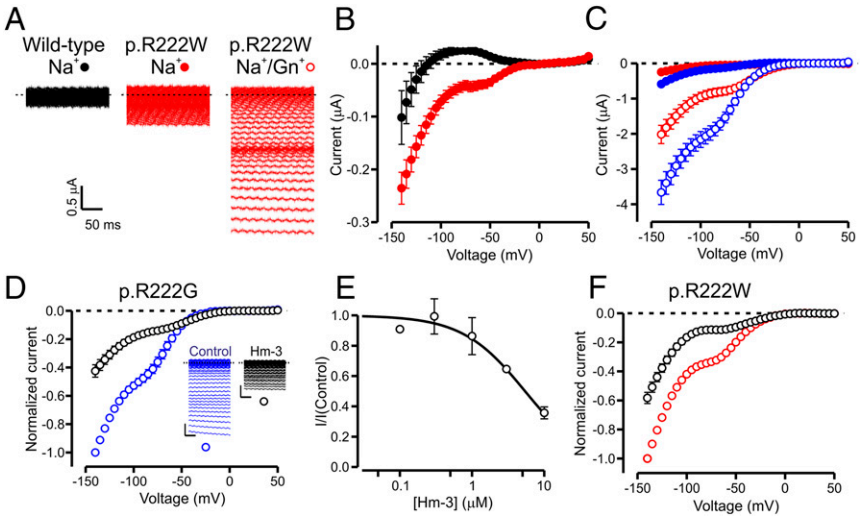

Fig. 2. Hm-3 inhibits I_{GP}s in p.R222W and p.R222G. (*A*) Representative current traces of wild-type or p.R222W channels in Na^+ or Na^+/Gn^+ solution. (*B*) I_{GP} of wild-type (black, $n = 20$) and p.R222W (red, $n = 21$) channels in Na^+ solution. (*C*) I_{GP} for p.R222W (red, $n = 21$) and p.R222G channels (blue, $n = 42$) in Na^+ (solid symbols) or Na^+/Gn^+ (open symbols) solution. (*D*) Current–voltage relationship of p.R222G I_{GP} in the absence (blue) or presence (black) of 10 μM Hm-3 ($n = 10$). (*Insets*) Representative current traces are shown. Data were normalized to current amplitude in response to a step to −140 mV in the absence of Hm-3. [Scale bars: 50 ms (x), 1 μA (y).] (*E*) Dose–response curve of p.R222G I_{GP} inhibition by Hm-3 at −80 mV ($n = 3$–10). I is the current measured in the presence of the Hm-3 concentration indicated in *x* axis. I(Control) is the current measured in its absence. (*F*) Current–voltage relationship of p.R222W I_{GP} in the absence (red) or presence (black) of 10 μM Hm-3 ($n = 4$). Data were normalized as in *D*. Error bars show SEM, and dashed lines indicate the zero current level. Voltage protocols are described in *SI Materials and Methods*.

We also asked if the inhibition of the I_{Na} by Hm-3 was affected by different VSD mutations (Fig. 3 *B*–*D* and Fig. S2 *A* and *B*). In response to voltage steps to −20 mV, inhibition by 1 μM Hm-3 was similar to wild-type for p.R672G and p.R1132Q channels. However, the reduction in current amplitude was significantly lower for p.R222G and p.R219G channels (for both mutants, $P < 0.01$ vs. wild-type channels). A nonsignificant trend toward a smaller effect on p.R222W and p.R225G was also seen. For p.R219G, p.R222G, and p.R225G, we also studied I_{Na} inhibition with 10 μM Hm-3, with both p.R222G and p.R219G showing reduced inhibition compared with wild-type channels ($P < 0.01$; Fig. 3*D*). Reduction in the inhibitory effect of Hm-3 on p.R222G channels is consistent with the higher IC_{50} of I_{GP} inhibition of p.R222G channels compared with the reported IC_{50} of I_{Na} inhibition of wild-type channels (27). A shift in the voltage dependence of activation by 10 μM Hm-3 was evident for p.R219G channels, although smaller than for wild-type channels. This indicates that the absence of inhibition of p.R219G I_{GP} by 10 μM Hm-3 is not due to a lack of Hm-3 binding to the channel. I_{Na} and I_{GP} data suggest that Hm-3 forms specific interactions with VSD-I. We proceeded to investigate this interaction using NMR spectroscopy.

Hm-3 Binds to the S3–S4 Helix–Loop–Helix Motif in VSD-I. VSD-I of human $Na_V1.4$ (residues L114–S246) was produced by cell-free expression (Fig. S3). Mixed micelles of zwitterionic detergents [1:1 dodecylphosphocholine/*N*,*N*-dimethyldodecylamine *N*-oxide (DPC/LDAO)] provided optimal conditions for NMR measurements (28). In this milieu, VSD-I has an expected α-helical content of ∼60% (Figs. S3*D* and S5*A*), but its stability at the temperatures needed for NMR studies is limited (half-lifetime of ∼24 h at 45 °C). Nevertheless, the backbone resonance assignment was obtained for ∼47% of residues belonging to the VSD sequence (Fig. 4*D* and Fig. S4*A*).

Hm-3 has previously shown affinity to zwitterionic and anionic lipid vesicles (27). We studied the interaction between Hm-3 and DPC/LDAO micelles in the absence of VSD-I (Fig. S4 *B* and *C*). The equilibrium dissociation constant of the Hm-3/micelle complex (K_M) of 36.5 ± 3.1 μM revealed that the toxin has a considerably high affinity to the micelle surface (Fig. S6*A*). Hm-3 interacts with the micelle through a hydrophobic cluster formed by aromatic residues (W11, F12, W16, and Y25), while positively and negatively charged groups either contact with polar head groups of detergents (e.g., K32) or protrude into the aqueous environment (Fig. 4*C* and Fig. S6 *B* and *D*). The spatial structure of the toxin does not change significantly upon micelle binding.

We then titrated ^{15}N-labeled VSD-I in DPC/LDAO micelles with unlabeled Hm-3 and vice versa. Changes in the position and intensities of the backbone $^1H^{15}N$ resonances (Fig. 4 *A* and *B* and Figs. S5*B* and S6*C*) indicated the formation of a toxin/channel complex and revealed the location of binding interfaces. Hm-3 interacts with the outer half of the S3 helix of VSD-I (S3b, residues S199–T207) and the C-terminal part of the S3–S4 extracellular loop (residues L212–I215) by the two-stranded, antiparallel β-sheet (residues C23–K28 and L31–I33) and W11 and

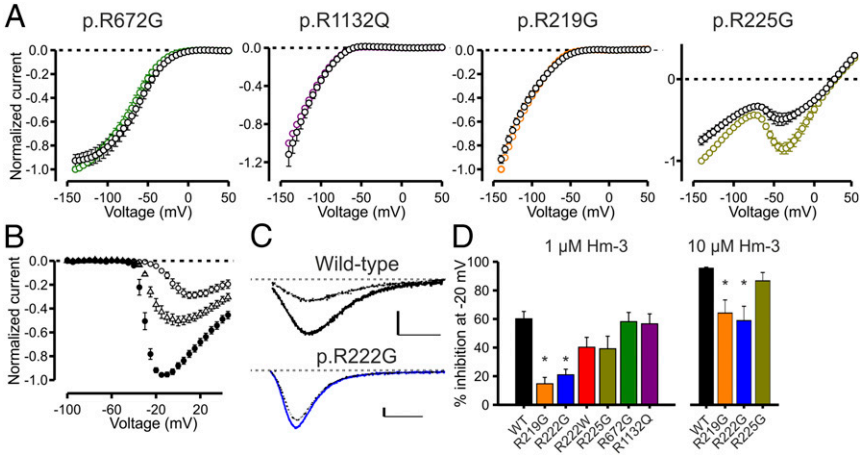

Fig. 3. VSD-I–specific action of Hm-3. (*A*) I_{GP} in the absence (colored symbols) and presence (black symbols) of 10 μM Hm-3 for S4 mutant channels (p.R672G: $n = 4$, p.R1132Q: $n = 4$, p.R219G: $n = 6$, and p.R225G: $n = 9$). Leak-subtracted data are shown for all but p.R225G, for which raw data are presented. Data were normalized to current amplitude in response to a step to −140 mV in the absence of Hm-3. (*B*–*D*) I_{Na} inhibition by Hm-3; the number of experiments is given in Fig. S2. (*B*) Current–voltage relationship for wild-type channels in the absence (●) and presence of 1 μM (△) or 10 μM (○) Hm-3. (*C*) Representative current traces in response to a voltage step to −20 mV in the absence (solid) and presence (dashed) of Hm-3 for wild-type and p.R222G channels. [Scale bars: 2 ms (*x*), 0.5 μA (*y*).] (*D*) Percentage of current inhibited by 1 μM (*Left*) and 10 μM (*Right*) Hm-3 at −20 mV for wild-type (black) and mutant channels (*$P < 0.01$). Error bars show SEM, and dashed lines indicate the zero current level.

F12 belonging to the membrane-binding surface (Fig. 4 *C* and *D*). The S3–S4 loop accommodates two negatively charged groups (E208 and D211). Although the signals of these residues are not identified in the NMR spectra, significant changes are observed for the neighboring residues T207 and L212, implying the participation of their side chains in complex formation. In contrast, the absence of any responses from residues A217 and R225 (R3) in the S4 helix indicates that they do not participate in toxin binding; R219 and R222 (R1 and R2) remained unassigned. The absence of chemical shift perturbations indicates that the binding of Hm-3 does not introduce significant changes in the spatial structure of VSD-I outside the S3b/S3–S4 loop and the topology of Hm-3/micelle interaction is not significantly altered upon toxin binding to VSD-I. The equilibrium dissociation constant of the Hm-3/VSD-I complex (K_D) of 6.2 ± 0.6 μM was determined by the analysis of VSD-I chemical shift changes during Hm-3 titration (Fig. S7 *C* and *D*). A pull-down assay using VSD-I attached to an Ni^{2+} resin confirmed the formation of the Hm-3/VSD-I complex (Fig. S7*F*).

To confirm that Hm-3 interacts with the S3–S4 helix–loop–helix ("paddle") motif of VSD-I, we tested the activity of Hm-3 on K_V2.1 channels where their paddle motif was substituted with the corresponding structures of Na_V1.4 VSDs (29). The activity of the resulting hybrid channels was significantly reduced by 1.5 μM Hm-3 only when the paddle motif of VSD-I was introduced (Fig. 4*E*), but not that of any other VSDs (n = 3). In addition, we replaced Na_V1.4 residues suggested by NMR to interact with Hm-3 (p.D211H and p.E208A). The inhibition of I_{Na} by 1 μM Hm-3 was reduced significantly in p.D211H (n = 6; Fig. S2 *A* and *B*), while a small nonsignificant reduction was observed in p.E208A (n = 9). At 10 μM, Hm-3 inhibition of p.D211H (n = 4) and p.E208A (n = 3) channels was wild-type–like (Fig. S2 *A* and *B*).

NMR-Based Model of Hm-3/VSD-I Complex. The Hm-3 complex with the up state of VSD-I was modeled using protein-to-protein docking with specific restraints imposed by NMR (Fig. S8). A resulting solution (Fig. 5*A*) shows the toxin peripherally attached to the S3b–S4 region of VSD-I. The complex is stabilized by two salt bridges (K24–E208 and K28–D211) and by hydrophobic/stacking interactions: W11 side chain is sandwiched between F198, I201, M202, and Y205; Y25 makes contacts with M202, M203, and L206; and I27 is in contact with L206 and I215. In addition, F209 of VSD-I may participate in hydrophobic interactions with I33 and V35 residues in the C-terminal β-strand of the toxin.

Discussion

VSD-I as a Binding Site for Gating Modifier Toxins. We present several lines of evidence that the crab spider toxin Hm-3 affects channel gating by interacting with VSD-I. Hm-3 inhibits I_{GP} evoked by mutations in VSD-I (Fig. 2 *D–F*), but not in VSD-II or VSD-III (Fig. 3*A*), and Hm-3 inhibition of I_{Na} is reduced by mutations of R1 and R2 in VSD-I, while unaffected by mutations of R2 in VSD-II or VSD-III (Fig. 3 *C* and *D*). In addition, Hm-3 alters NMR signals in the paddle motif of VSD-I (Fig. 4*D*), and when this region is inserted in K_V2.1 channels, it conveys Hm-3 sensitivity to these channels (Fig. 4*E*). Finally, a mutation in the VSD-I S3–S4 loop predicted to break a salt bridge reduces the inhibitory effect of Hm-3 (Fig. S2 *A* and *B*). VSD-I has been proposed as one of the binding sites for ProTx-II from the tarantula *Thrixopelma pruriens*, but it is not the principal site (30, 31). We therefore identify VSD-I as a specific binding site for gating modifier toxins (Fig. 5*B*).

Hm-3 inhibits Na_V1.4 at submicromolar concentrations but does not affect all Na_V isoforms (27). Alignment of the proposed binding site shows that the S3–S4 loop is one of the most variable regions of VSD-I (Fig. S9), and some of the nonsensitive isoforms lack the aspartate corresponding to D211 (Na_V1.2 and Na_V1.3) or a hydrophobic residue corresponding to M203 (Na_V1.1). These residues form contacts with Hm-3 in our model (Fig. 5*A*). Another Hm-3–resistant channel, Na_V1.8, contains an additional positively charged residue in the S3–S4 loop. In agreement with our mutagenesis data, E208 is missing in the insect $DmNa_V$1 channel, which is sensitive to Hm-3.

NMR data suggest that Hm-3 can anchor onto the membrane surface in a position compatible with binding the paddle motif (Figs. 4*C* and 5 *A* and *B*). A similar mechanism was proposed for some other gating modifier toxins from spider venom acting on K_V and Na_V channels (e.g., VsTx1, ProTx-II, huwentoxin-IV, SgTx1,

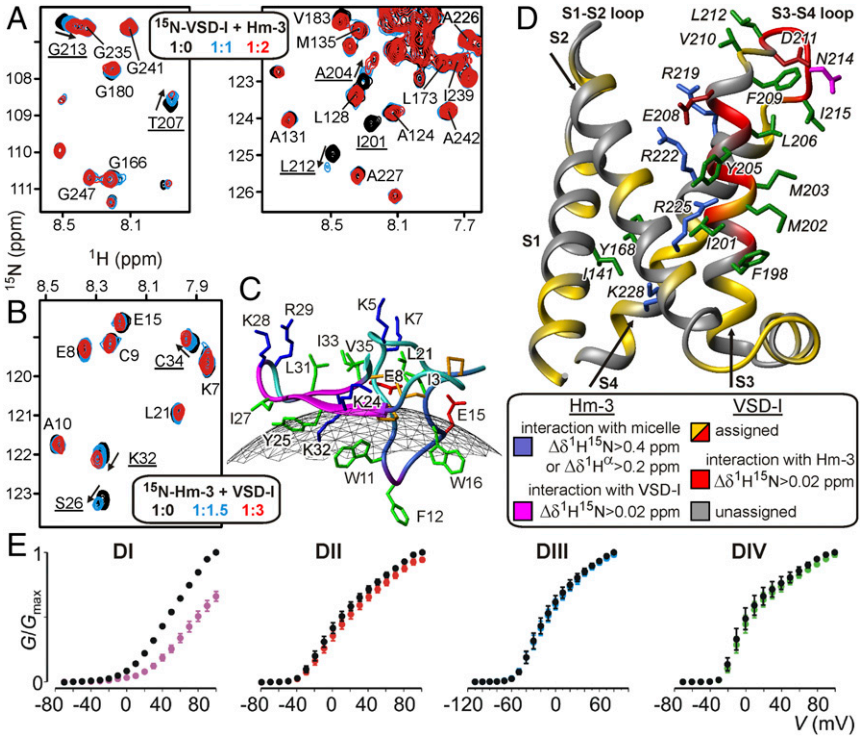

Fig. 4. Hm-3/VSD-I interaction interface. (*A* and *B*) Superposition of ^1H,^{15}N-TROSY spectra of VSD-I and Hm-3 at different VSD-I/Hm-3 molar ratios. (*C*) Interfaces of Hm-3 interaction with the micelle (blue) and VSD-I (magenta) are mapped on the Hm-3 structure. Disulfide bonds are colored in yellow. Gray mesh shows the approximate micelle surface with a radius of ~24 Å. (*D*) Interface of VSD-I interaction with Hm-3 is mapped on a homology model of VSD-I. The side chains forming the interaction interface are annotated. The conserved Arg/Lys residues of the S4 helix are also shown. Hydrophobic aliphatic and aromatic residues, polar uncharged, positively charged, and negatively charged residues are colored in green, magenta, blue, and red, respectively. (*E*) Conductance–voltage relationships for the chimeric K_V2.1 constructs containing the S3–S4 helix–loop–helix motif of one of the four Na_V1.4 VSDs before (black) and following (colored) addition of 1.5 μM Hm-3 (n = 3 each, error bars show SEM). D, domain; G is the conductance measured at the voltage indicated in x axis, G_{max} is the normalized maximal conductance measured in control condition.

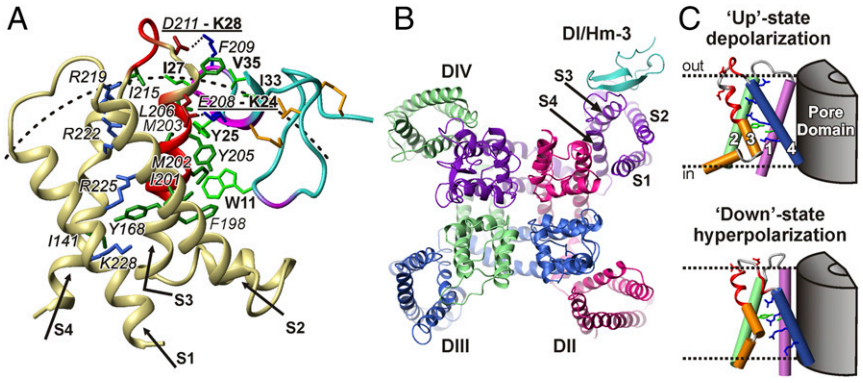

Fig. 5. Mode of Hm-3 action on I_{GP}. (*A*) Model of the Hm-3/VSD-I complex. The backbones of fragments that participate in the formation of interaction surfaces are colored in red (VSD-I) and magenta (Hm-3). The charged and hydrophobic side chains at the interface are annotated. Salt bridges are shown by dotted lines. The micelle surface is shown by a dashed line. (*B*) Position of Hm-3 relative to the full-length α-subunit of Na_V channel. (*C*) VSD-I of $Na_V1.4$ channel modeled in the up and down states. The Hm-3 binding regions are colored red. Negatively and positively charged residues of the S3–S4 loop and S4 are colored red and blue, respectively. D, domain.

GxTx-1E) (32). Hm-3 binds to the channel with its β-hairpin, interacting with negatively charged residues from the S3–S4 loop (Fig. 5*A*); such residues in the same loop of other VSDs are essential for binding of other toxins (32–35) (Fig. 1*C*). Our model of the Hm-3/VSD-I complex is in good agreement with the model describing interactions of spider gating modifier toxins with K_V channels (32, 34, 36, 37).

Hm-3 Mode of Action. Several lines of evidence suggest that Hm-3 stabilizes the down state of VSD-I: (*i*) the toxin inhibits $Na_V1.4$ I_{Na} by shifting channel activation to more positive voltages (27), (*ii*) Hm-3 inhibits the hyperpolarization-activated I_{GP} of p.R222G/W channels (Fig. 2 *D*–*F*), (*iii*) Hm-3 shifts the voltage dependence of p.R222G I_{GP} to more depolarized voltages (Fig. S2*C*), and (*iv*) Hm-3 inhibits the depolarization-activated p.R225G I_{GP} similar to I_{Na}: Conductance increases at more positive voltages (Fig. 3*A*). However, Hm-3 does not alter the voltage dependence of p.R219G I_{GP} in contrast to I_{Na}. This may be due to the reduced shift of p.R219G I_{Na} by Hm-3 and the fact that its I_{GP} is activated at more hyperpolarized voltages than p.R222G I_{GP} (Fig. 2*C* vs. 3*A*).

Our NMR data likely describe the up state of VSD-I as the recordings were made in the absence of voltage. This suggests that similar to other gating modifier toxins from spider venom (38), Hm-3 interacts with both up and down states of VSD-I but has a higher affinity to the down state. Indeed, Hm-3 inhibition of I_{Na} (27) and I_{GP} (Fig. S2*D*) can be reversed by applying prolonged depolarizing voltage pulses. At a constant tail voltage of −100 mV, inhibition by Hm-3 is at its maximum following hyperpolarizing prepulses. However, after depolarizing prepulses the tail current amplitude increases, suggesting that the inhibition by the toxin is relieved when the voltage sensor moves to the up state.

Binding of Hm-3 to the up state is likely to be membrane-mediated. A major free energy contribution to the stability of the Hm-3/VSD-I complex comes from the partition of the toxin into the micelle (free energy of −6.5 kcal/M; Fig. S7*E*), while binding to VSD-I within the micelle adds only −1.1 kcal/M. However, this comparatively low free energy gain does not necessarily indicate the weakness of the toxin/domain complex. It rather suggests that Hm-3 forms hydrophobic and electrostatic contacts similar to those already present between VSD-I and lipids.

Currently, high-resolution structural data of ion channel VSDs are available only for the up state. Consequently, the binding of Hm-3 to the down state of VSDs cannot be modeled accurately. It is evident, however, that the relative orientation of Hm-3 binding elements, the S3b helix and S3–S4 loop, changes from two spatially separated regions in the up-state models to a continuous surface in the down-state models of VSDs (39) (Fig. 5*C*). This compaction of the binding interface likely underlies the increased affinity of the toxin to the resting state.

Our data suggest that stabilization of the voltage sensor by Hm-3 in the down state does not, per se, result in the inhibition of p.R222G/W I_{GP}. Rather, by preventing the up movement of S4 in VSD-I, Hm-3 stabilizes the active state of I_{GP} (Fig. S2*C*). Our data also suggest that Hm-3 forms specific and state-dependent interactions to inhibit I_{GP}. We propose that Hm-3 stabilizes VSD-I in the down state where p.R222G I_{GP} is active. Hm-3 either introduces a local conformational change sufficient to constrict the gating pore or directly occludes it. The reduced I_{Na} inhibition of R1 and R2 mutant channels by Hm-3 suggests that it may directly interact with these residues in the down state and, in the absence of R2, prevent the flow of ions through the gating pore.

Toxins as Hits for Development of HypoPP Therapies. The main pathomechanism of HypoPP is presumed to consist of gating pore leak currents through VSDs of $Na_V1.4$ or $Ca_V1.1$ that depolarize and paralyze the muscle. Thus, compounds blocking the leak currents may prevent the depolarization and paralysis. We identify the gating modifier toxin Hm-3 as an inhibitor of I_{GP} of HypoPP p.R222G/W channels. Hm-3 also suppresses I_{Na} of wild-type and mutant channels, limiting its clinical usefulness. However, our study proposes several ways forward to develop agents with improved selectivity toward I_{GP} and with minimum activity on the wild-type channel. First, gating modifier toxins are a useful source for identifying novel I_{GP} inhibitors. Second, application of guanidinium will increase the throughput of I_{GP} pharmacological studies, allowing characterization of a large number of toxins on a set of mutant VSDs. Finally, NMR studies can identify key toxin–channel interactions that may help direct the development of hit compounds, clarify the pharmacophores, and eventually improve the therapeutic options of HypoPP.

Materials and Methods

Hm-3 Production. Hm-3 was produced recombinantly following a published procedure (27) as part of a fusion protein with thioredoxin, which was cleaved at methionine residues by cyanogen bromide (40). For NMR studies, ^{15}N-labeled Hm-3 was produced. In this case, transformed *Escherichia coli* cells were first cultured in LB medium. Having reached the mid-log phase, the cells were pelleted and resuspended in the minimal growth medium M9 containing 1 mM $MgSO_4$, 0.1 mM $CaCl_2$, 0.2% glucose, 0.1% $^{15}NH_4Cl$, 0.6% NaH_2PO_4, 0.3% K_2HPO_4, 0.05% NaCl, and 1 mM thiamine (pH 7.0). All other steps were carried out as with cold toxin.

Molecular Biology and Electrophysiology. Materials and methods for mutagenesis, the $Na_V1.4$ channel patch clamp in HEK293 cells, and the two-electrode voltage clamp of *X. laevis* are described by Zaharieva et al. (16) and in *SI Materials and Methods*. Chimeric rat $Na_V1.4/K_V2.1$ constructs were generated as described by Bosmans et al. (29).

Oocytes for $Na_V1.4$ expression work were isolated from adult female *X. laevis* in accordance with the UK Animal (Scientific Procedures) Act 1986 or the Animal Care and Use Committee of Johns Hopkins University.

VSD-I Sample Preparation and NMR Spectroscopy. Samples of the unlabeled and ^{15}N- and $^{13}C,^{15}N$-labeled VSD-I were produced using a cell-free expression system in the insoluble form as described elsewhere (28, 41). The precipitate of the reaction mixture was solubilized in 500 μL of 20 mM Tris·HCl, 300 mM NaCl, and 10% DPC (pH 8.0), and purified by Ni^{2+} chromatography in 0.5% DPC. LDAO was added to the purified protein (*SI Materials and Methods*).

NMR spectra were recorded on Bruker Avance-III 600 and 800 spectrometers equipped with cryoprobes at pH 5.5 and 45 °C. $^{1}H,^{15}N$-TROSY spectra were used to monitor binding of Hm-3 to ^{15}N-labeled VSD-I and vice versa. Detergent concentration in the samples was kept constant during titrations. Equilibrium dissociation constants of Hm-3/micelle and Hm-3/VSD-I complexes (K_M and K_V, respectively) were determined from the chemical shift titration data assuming fast (on the NMR time scale) exchange of Hm-3 molecules between three different states (Fig. S7*E*).

Computer Modeling. Homology models of VSD-I in the up and down states were constructed using as a template the VSD-I from the cryo-EM structure of the Na_VPaS channel (42) and the structures from the molecular dynamics (MD) trajectory of the $K_V1.2/2.1$ chimeric channel (39), respectively. The recently published cryo-EM structure of the $Na_V1.4$ channel from the electric eel was not used for the modeling because VSD-I is poorly resolved in this structure (43). The structural model of the Hm-3/VSD-I complex was generated with the HADDOCK2.2 web server (44).

ACKNOWLEDGMENTS. We thank Stephen C. Cannon (University of California, Los Angeles), Kenton J. Swartz (National Institute of Neurological Disorders and Stroke/NIH) and Baron Chanda (University of Wisconsin–Madison) for sharing the expression clones, as well as David E. Shaw (D. E. Shaw Research) for providing models of the $K_V1.2/2.1$ channel in different states and Nikolay Petrosian for modelling VSD-I of $Na_V1.4$. This work was funded, in part, by UK Medical Research Council Project Grant MR/M006948/1 (to R.M.), the Wellcome Trust (D.A.K. and D.M.K.), the Molecular and Cell Biology Program of the Russian Academy of Sciences (A.A.V. and Z.O.S.), and Russian Foundation for Basic Research Grant 16-34-01185 (to A.A.B.). NMR study was funded by Russian Science Foundation Grant 16-14-10338 (to Z.O.S.). NMR experiments were carried out using equipment provided by the core facility of the Shemyakin–Ovchinnikov Institute of Bioorganic Chemistry (supported by Russian Ministry of Education and Science Grant RFMEFI62117X0018). Parts of this work were supported by NIH Grant R01NS091352 (to F.B.). M.G.T. was funded by an MRC Centre for Neuromuscular Diseases PhD studentship. M.G.T., M.G.H., and R.M. are supported by the University College London Hospitals Biomedical Research Centre. We dedicate this paper to the memory of Professor Eugene Grishin under whose leadership the study of *Heriaeus* toxins has begun.

1. Suetterlin K, Männikkö R, Hanna MG (2014) Muscle channelopathies: Recent advances in genetics, pathophysiology and therapy. *Curr Opin Neurol* 27:583–590.
2. Cavel-Greant D, Lehmann-Horn F, Jurkat-Rott K (2012) The impact of permanent muscle weakness on quality of life in periodic paralysis: A survey of 66 patients. *Acta Myol* 31:126–133.
3. Matthews E, et al. (2011) Acetazolamide efficacy in hypokalemic periodic paralysis and the predictive role of genotype. *Neurology* 77:1960–1964.
4. Jurkat-Rott K, et al. (2009) K+-dependent paradoxical membrane depolarization and Na+ overload, major and reversible contributors to weakness by ion channel leaks. *Proc Natl Acad Sci USA* 106:4036–4041.
5. Matthews E, et al. (2009) Voltage sensor charge loss accounts for most cases of hypokalemic periodic paralysis. *Neurology* 72:1544–1547.
6. Cannon SC (2010) Voltage-sensor mutations in channelopathies of skeletal muscle. *J Physiol* 588:1887–1895.
7. Catterall WA (2012) Voltage-gated sodium channels at 60: Structure, function and pathophysiology. *J Physiol* 590:2577–2589.
8. Yang N, Horn R (1995) Evidence for voltage-dependent S4 movement in sodium channels. *Neuron* 15:213–218.
9. Starace DM, Bezanilla F (2004) A proton pore in a potassium channel voltage sensor reveals a focused electric field. *Nature* 427:548–553.
10. Tombola F, Pathak MM, Isacoff EY (2005) Voltage-sensing arginines in a potassium channel permeate and occlude cation-selective pores. *Neuron* 45:379–388.
11. Jurkat-Rott K, Groome J, Lehmann-Horn F (2012) Pathophysiological role of omega pore current in channelopathies. *Front Pharmacol* 3:112.
12. Sokolov S, Scheuer T, Catterall WA (2007) Gating pore current in an inherited ion channelopathy. *Nature* 446:76–78.
13. Struyk AF, Cannon SC (2007) A Na+ channel mutation linked to hypokalemic periodic paralysis exposes a proton-selective gating pore. *J Gen Physiol* 130:11–20.
14. Struyk AF, Markin VS, Francis D, Cannon SC (2008) Gating pore currents in DIIS4 mutations of NaV1.4 associated with periodic paralysis: Saturation of ion flux and implications for disease pathogenesis. *J Gen Physiol* 132:447–464.
15. Francis DG, Rybalchenko V, Struyk A, Cannon SC (2011) Leaky sodium channels from voltage sensor mutations in periodic paralysis, but not paramyotonia. *Neurology* 76: 1635–1641.
16. Zaharieva IT, et al. (2016) Loss-of-function mutations in SCN4A cause severe foetal hypokinesia or 'classical' congenital myopathy. *Brain* 139:674–691.
17. Groome JR, et al. (2014) NaV1.4 mutations cause hypokalaemic periodic paralysis by disrupting IIIS4 movement during recovery. *Brain* 137:998–1008.
18. Habbout K, et al. (2016) A recessive Nav1.4 mutation underlies congenital myasthenic syndrome with periodic paralysis. *Neurology* 86:161–169.
19. Sokolov S, Scheuer T, Catterall WA (2008) Depolarization-activated gating pore current conducted by mutant sodium channels in potassium-sensitive normokalemic periodic paralysis. *Proc Natl Acad Sci USA* 105:19980–19985.
20. Catterall WA, et al. (2007) Voltage-gated ion channels and gating modifier toxins. *Toxicon* 49:124–141.
21. Carle T, et al. (2006) Gating defects of a novel Na+ channel mutant causing hypokalemic periodic paralysis. *Biochem Biophys Res Commun* 348:653–661.
22. Jurkat-Rott K, et al. (2000) Voltage-sensor sodium channel mutations cause hypokalemic periodic paralysis type 2 by enhanced inactivation and reduced current. *Proc Natl Acad Sci USA* 97:9549–9554.
23. Kuzmenkin A, et al. (2002) Enhanced inactivation and pH sensitivity of Na(+) channel mutations causing hypokalaemic periodic paralysis type II. *Brain* 125:835–843.
24. Rüdel R, Lehmann-Horn F, Ricker K, Küther G (1984) Hypokalemic periodic paralysis: In vitro investigation of muscle fiber membrane parameters. *Muscle Nerve* 7:110–120.
25. Sokolov S, Scheuer T, Catterall WA (2010) Ion permeation and block of the gating pore in the voltage sensor of NaV1.4 channels with hypokalemic periodic paralysis mutations. *J Gen Physiol* 136:225–236.
26. Nikolsky AS, et al. (2009) Voltage-gated sodium channels are targets for toxins from the venom of the spider Heriaeus melloteei. *Biochem (Mosc) Suppl Ser A Membr Cell Biol* 3:245–253.
27. Berkut AA, et al. (2015) Structure of membrane-active toxin from crab spider Heriaeus melloteei suggests parallel evolution of sodium channel gating modifiers in Araneomorphae and Mygalomorphae. *J Biol Chem* 290:492–504.
28. Myshkin MY, et al. (2017) "Divide and conquer" approach to the structural studies of multidomain ion channels by the example of isolated voltage sensing domains of human Kv2.1 and Nav1.4 channels. *Russ J Bioorg Chem* 43:634–643.
29. Bosmans F, Martin-Eauclaire MF, Swartz KJ (2008) Deconstructing voltage sensor function and pharmacology in sodium channels. *Nature* 456:202–208.
30. Xiao Y, Blumenthal K, Cummins TR (2014) Gating-pore currents demonstrate selective and specific modulation of individual sodium channel voltage-sensors by biological toxins. *Mol Pharmacol* 86:159–167.
31. Das S, Gilchrist J, Bosmans F, Van Petegem F (2016) Binary architecture of the Nav1.2-β2 signaling complex. *eLife* 5:e10960.
32. Milescu M, et al. (2009) Interactions between lipids and voltage sensor paddles detected with tarantula toxins. *Nat Struct Mol Biol* 16:1080–1085.
33. Cai T, et al. (2015) Mapping the interaction site for the tarantula toxin hainantoxin-IV (β-TRTX-Hn2a) in the voltage sensor module of domain II of voltage-gated sodium channels. *Peptides* 68:148–156.
34. Swartz KJ, MacKinnon R (1997) Hanatoxin modifies the gating of a voltage-dependent K+ channel through multiple binding sites. *Neuron* 18:665–673.
35. Xiao Y, Jackson JO, 2nd, Liang S, Cummins TR (2011) Common molecular determinants of tarantula huwentoxin-IV inhibition of Na+ channel voltage sensors in domains II and IV. *J Biol Chem* 286:27301–27310.
36. Tao H, et al. (2013) Analysis of the interaction of tarantula toxin Jingzhaotoxin-III (β-TRTX-Cj1α) with the voltage sensor of Kv2.1 uncovers the molecular basis for cross-activities on Kv2.1 and Nav1.5 channels. *Biochemistry* 52:7439–7448.
37. Alabi AA, Bahamonde MI, Jung HJ, Kim JI, Swartz KJ (2007) Portability of paddle motif function and pharmacology in voltage sensors. *Nature* 450:370–375.
38. Phillips LR, et al. (2005) Voltage-sensor activation with a tarantula toxin as cargo. *Nature* 436:857–860.
39. Jensen MO, et al. (2012) Mechanism of voltage gating in potassium channels. *Science* 336:229–233.
40. Andreev YA, Kozlov SA, Vassilevski AA, Grishin EV (2010) Cyanogen bromide cleavage of proteins in salt and buffer solutions. *Anal Biochem* 407:144–146.
41. Paramonov AS, et al. (2017) NMR investigation of the isolated second voltage-sensing domain of human Nav1.4 channel. *Biochim Biophys Acta* 1859:493–506.
42. Shen H, et al. (2017) Structure of a eukaryotic voltage-gated sodium channel at near-atomic resolution. *Science* 355:eaal4326.
43. Yan Z, et al. (2017) Structure of the Nav1.4-beta1 complex from electric eel. *Cell* 170: 470–482.e11.
44. van Zundert GCP, et al. (2016) The HADDOCK2.2 web server: User-friendly integrative modeling of biomolecular complexes. *J Mol Biol* 428:720–725.